Actin and microtubules in bristle elongation

Regulation of TGF-β signalling

Chromosome condensation induced by geminivirus infection of mature plant cells

Hank W. Bass[1,2], Steven Nagar[3], Linda Hanley-Bowdoin[4] and Dominique Robertson[3,*]

[1]Department of Biological Science, Florida State University, Tallahassee, FL 32306-4370, USA (bass@bio.fsu.edu)
[2]Department of Molecular and Cell Biology, University of California, Berkeley, USA
[3]Department of Botany, North Carolina State University, Raleigh, NC 27695-7612, USA
[4]Department of Biochemistry, North Carolina State University, Raleigh, NC 27695-7622, USA
*Author for correspondence (e-mail: niki_robertson@ncsu.edu)

SUMMARY

Tomato golden mosaic virus (TGMV) is a geminivirus that replicates its single-stranded DNA genome through double-stranded DNA intermediates in nuclei of differentiated plant cells using host replication machinery. We analyzed the distribution of viral and plant DNA in nuclei of infected leaves using fluorescence in situ hybridization (FISH). TGMV-infected nuclei showed up to a sixfold increase in total volume and displayed a variety of viral DNA accumulation patterns. The most striking viral DNA patterns were bright, discrete intranuclear compartments, but diffuse nuclear localization was also observed. Quantitative and spatial measurements of high resolution 3-dimensional image data revealed that these compartments accounted for 1-18% of the total nuclear volume or 2-45% of the total nuclear FISH signals. In contrast, plant DNA was concentrated around the nuclear periphery. In a significant number of nuclei, the peripheral chromatin was organized as condensed prophase-like
fibers. A combination of FISH analysis and indirect immunofluorescence with viral coat protein antibodies revealed that TGMV virions are associated with the viral DNA compartments. However, the coat protein antibodies failed to cross react with some large viral DNA inclusions, suggesting that encapsidation may occur after significant viral DNA accumulation. Infection by a TGMV mutant with a defective coat protein open reading frame resulted in fewer and smaller viral DNA-containing compartments. Nevertheless, nuclei infected with the mutant virus increased in size and in some cases showed chromosome condensation. Together, these results established that geminivirus infection alters nuclear architecture and can induce plant chromatin condensation characteristic of cells arrested in early mitosis.

Key words: Geminivirus, DNA replication, Chromosome condensation, 3-D deconvolution

INTRODUCTION

Geminiviruses are a family of single-stranded DNA viruses that replicate by means of a rolling circle mechanism in plant nuclei (Hanley-Bowdoin et al., 1999; Laufs et al., 1995). Tomato golden mosaic virus (TGMV), a member of the begomovirus subgroup, infects species in the Solanaceae including petunia, *Datura*, and *Nicotiana benthamiana*, a tobacco relative commonly used as its host. The TGMV genome consists of two circular molecules called the A and B components, each about 2.5 kb in size (Hamilton et al., 1984). The A component encodes all the viral proteins required for replication and encapsidation (Rogers et al., 1986; Sunter et al., 1987). The B component specifies proteins necessary for cell-to-cell movement and symptom development (Sunter et al., 1987). Viral single-stranded DNA (ssDNA) is encapsidated into twin icosahedral particles by the AR1 or coat protein, which is dispensable for infection of *N. benthamiana* but required for insect transmission (Brough et al., 1988; Gardiner et al., 1988; Pooma et al., 1996). Previous studies showed that

virions can form large crystalline arrays in nuclei of a variety of *N. benthamiana* cell types, including epidermal, mesophyll and vascular tissue (Rushing et al., 1987). A double-stranded form of TGMV DNA is also present in infected cells (Bisaro et al., 1982), where it serves as template for viral replication and transcription.

Geminiviruses do not encode their own DNA polymerase and, instead, rely on host DNA replication machinery. In a previous study, we showed that TGMV causes the accumulation of the host DNA synthesis protein, proliferating cell nuclear antigen (PCNA), in infected nuclei of differentiated cells (Nagar et al., 1995). PCNA is an accessory factor for DNA polymerase delta and is associated with both DNA replication and repair in mammalian cells (Bravo et al., 1987; Kelman, 1997). Analysis of transgenic plants that constitutively express the TGMV replication protein, AL1, demonstrated that this viral protein is sufficient to induce PCNA expression in differentiated cells (Nagar et al., 1995). Experiments showing that AL1 interacts with a plant homologue to the animal tumor suppressor protein,

retinoblastoma (Ach et al., 1997; Collin et al., 1996; Xie et al., 1995), suggested that like mammalian DNA tumor viruses, geminiviruses modify cell cycle controls to induce differentiated cells to reenter S phase.

Several studies have established that mammalian DNA viruses replicate in discrete nuclear compartments associated with DNA synthesis (de Bruyn Kops and Knipe, 1994; Ishov and Maul, 1996; Ishov et al., 1997; Uprichard and Knipe, 1997). In contrast, little is known about plant nuclear architecture and DNA virus replication. To date, the only studies describing the location of geminivirus accumulation within nuclei have relied on methods for detecting virions, which may not fully reflect the distribution of viral DNA (Kim et al., 1978; Rushing et al., 1987). To address this limitation and to improve understanding of the relationship between geminivirus and plant DNA replication, we used high-resolution, fluorescence in situ hybridization (FISH) and three-dimensional reconstructions to analyze and compare the distributions of TGMV and host DNA in infected nuclei.

MATERIALS AND METHODS

Plant inoculation

Nicotiana benthamiana plants were grown at 25°C, 65% humidity, in a 14-hour light/10-hour dark photoperiod. Plants at the 4 to 6 expanded leaf stage were bombarded by means of a Biolistic PDS 1000/He system (Bio-Rad, Hercules, CA) as described elsewhere (Nagar et al., 1995). For bombardment, 1.0 μm gold microprojectiles were coated with plasmid DNA (5 μg of each plasmid) containing partial tandem dimers of the wild-type TGMV A (pTG1.3A) and TGMV B (pTG1.4B; Fontes et al., 1994). The coat protein mutant was inoculated similarly with a TGMV A plasmid containing a frameshift near the 5′ end of the AR1 gene (Pooma et al., 1996). Tissues were harvested from systemically infected plants 11-14 days post inoculation (d.p.i.).

Fixation and sectioning of plant tissues

Leaf tissue was fixed for 3-5 hours at 25°C in chromatin-preserving buffer AN (15 mM PIPES, pH 6.8, 80 mM KCl, 20 mM NaCl, 0.5 mM EDTA, 2.0 mM EGTA, 0.15 mM spermine, 0.5 mM spermidine, 1.0 mM DTT and 0.01 mM sodium acetate) containing 4% formaldehyde (modified from Belmont et al., 1989). Tissues were then washed 30 minutes in several changes of buffer AN and stored at 4°C. Fixed tissues were embedded in 5% low-gelling-temperature agarose (Type XI, Sigma, St Louis, MO) in distilled water, and 50-60 μm sections cut with a Vibratome 1000 (Technical Products International, Inc., St Louis, MO).

Fluorescence in situ hybridization

We subjected fixed leaf sections to polyacrylamide FISH for 3-D imaging as previously described (Bass et al., 1997) using fluorescent oligonucleotides that specifically detected TGMV DNA. Each 30-nt probe was co-synthetically labeled at its 5′ end by '10 O.D. standard synthesis', but with an additional HPLC purification for the Texas Red-labeled probes (GENSET Corp., Paris, France). Probes were named to indicate the genome (A or B, Fig. 1) and the strand, plus (P) or minus (M), from which they were derived. For example, the probe AM, had sequence derived from the minus strand of the A component and hybridized to plus strand DNA. The DNA sequences were AM: 5′-CGTTTCCAAGTGATCCACAGGTTTCACGCC-3′; AP: 5′-AACCATGGCTTCCTCCGTTCCACGTCTCAT-3′; BM: 5′-CGTGTGCACGTTGATCTTAGCATGGATGGG-3′; and BP: 5′-AACGCAACAGGATCCGTGGTCGTGGAGATT-3′.

Total plant DNA from *N. benthamiana* was purified by cesium chloride density centrifugation and 1.3 μg was fluorescently labeled with FluoroRed dUTP (0.05 mM, Amersham Pharmacia, Upsala, Sweden) using a random primer labeling kit (Roche Biochemicals, Ind. IN). A 30 μl probe mix contained ~300 ng fluorescent *N. benthamiana* DNA in 2× SSC and 50% deionized formamide.

Three-dimensional microscopy, image processing and analysis

We recorded The 3-D images (Figs 2-7) using an Olympus IMT-2 wide-field microscope equipped with an oil-immersion lens (×60 NA 1.4 PlanApo, Olympus) (Hiraoka et al., 1991). The data were oversampled in the X, Y, and Z dimensions (XYZ voxel dimensions of $0.11 \times 0.11 \times 0.3$ μm^3) with the deconvolution light microscope workstation. Initial data were collected by CCD imaging over large areas of the leaf sections, followed by 3-D iterative deconvolution (Chen et al., 1995). The resulting large data sets were then cropped around individual whole nuclei for analysis and display. The images were adjusted for brightness and contrast by linear scaling, and multiple wavelength images were pseudocolored. Through-focus projections were made under the 'display maximum intensity' option.

Datasets containing 3-D images of individual nuclei were interactively modeled with Priism software (IVE3.2 and IVE3.3, D. A. Agard and J. W. Sedat, University of California, San Francisco) to extract spatial and quantitative data on the nuclear substructures (Chen et al., 1996). The EditPolygon program was used to trace the edges of the nucleus (DAPI image) or the edges of the intranuclear compartments delineated by the TGMV FISH signals. The polygon series were connected into 3-D, continuous surface objects with the VolumeBuilder program. Once modeled, the nucleus was partitioned into two sections – within or not within the FISH-stained intranuclear compartments. This method was used to determine the proportion of volume and FISH signals corresponding to the intranuclear compartments (Table 1).

Immunolocalization of TGMV coat protein

All incubations were performed at 25°C. Following in situ hybridization, sections were transferred to 1× PBS, pH 7.4, containing 0.1% BSA (PBS-BSA). Sections were blocked in 10% goat serum (Sigma, St Louis, MO) in PBS-BSA for 1 hour. After a 5 minute wash in PBS-BSA, sections were incubated for 1 hour with anti-coat protein monoclonal antibodies diluted 1:5 in PBS-BSA. After three 10-minute washes in PBS-BSA, sections were incubated for 1 hour with an Alexa 488-conjugated goat anti-mouse secondary antibody (Molecular Probes, Eugene, OR) diluted 1:250 in PBS-BSA. After three 10-minute washes in PBS-BSA, sections were mounted on slides in 90% glycerol in 1× PBS containing 1 μg/ml DAPI. Images were recorded on Kodak Elite film ASA 400 with a Nikon Eclipse 800 fluorescence microscope.

RESULTS

Cellular architecture is preserved during FISH

Previous ultrastructural analyses established that TGMV-infected nuclei with large inclusion bodies also accumulate DNA at their periphery (Rushing et al., 1987). It was not known whether they did so as a consequence of a deteriorated nuclear architecture because of viral packaging or a requirement for viral DNA synthesis. To examine the geminivirus-induced reorganization of the nucleus, we generated a series of fluorescent oligonucleotide probes that selectively visualize minus- and plus-strands of TGMV DNA in direct-labeled FISH experiments. The hybridization position of each probe in the TGMV genome is shown in Fig. 1. Probes corresponding to minus strand (AM and BM) hybridize to both
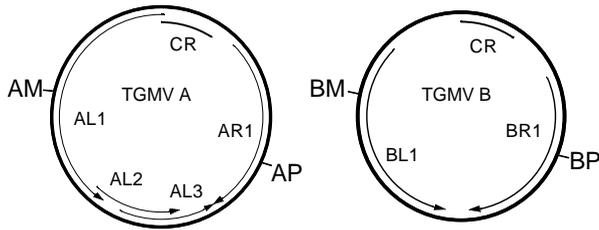
Fig. 1. Plus and minus strand probes for hybridization. The TGMV genome comprises two circular molecules, TGMV A and B. The AP probe hybridizes to dsDNA and has the same polarity as AL1 mRNA. AM hybridizes to ssDNA and dsDNA from the TGMV A component. The BP and BM probes hybridize to minus (dsDNA only) and plus strand DNA, respectively. CR, common region, a 200 bp sequence containing the origin of replication. AL1, AL2, and AL3 encode proteins needed for replication and transcription. AR1 is the viral coat protein. BR1 and BL1 are needed for cell-to-cell and long distance movement.

Mature, differentiated tissue of intact *N. benthamiana* plants were bombarded with plasmids containing partial tandem repeats of the wild-type TGMV A and B components that support replicative release of unit-length viral DNA and infection (Elmer et al., 1988; Nagar et al., 1995). Systemically infected tissue was harvested approximately two weeks after bombardment, fixed and analyzed by 3-D FISH using multiple wavelength deconvolution microscopy (Bass et al., 1997). The resulting 3-D data sets consisted of three different images per optical section: (1) a DAPI-stained image that visualized viral DNA and chromatin, (2) an autofluorescent FITC image that visualized cell and tissue structure, and (3) a Texas Red FISH image that detected viral DNA.

As shown in Fig. 2, typical sections from systemically infected tissue contain a mixture of healthy and virus-infected cells. Healthy palisade parenchyma cells subjected to FISH (Fig. 2A) had densely packed plastids and nuclei at their edges. TGMV-infected cells (Fig. 2B-E) were less well structured and contained fewer plastids. Infected nuclei were enlarged and more centrally located in the cell. Healthy cells with normal morphology frequently adjoined infected cells. In Fig. 2C-D, the infected mesophyll nucleus (double arrows) was enlarged and contained numerous bright intranuclear compartments that stained with the Texas Red FISH probe (AM + BM, Fig. 2E). In contrast, the adjacent healthy nucleus (single arrow) was of normal size and did not show Texas Red signal above background (Fig. 2E). These results established that the disrupted nuclear morphology associated with TGMV infection was not due to experimental conditions, or to a general degradation of all cells in infected plants and that cell and tissue morphology were preserved after acrylamide FISH (Fig. 2A).

ssDNA and dsDNA forms of viral DNA, whereas probes corresponding to plus strand (AP and BP) hybridized to minus strand DNA, which is believed to be found exclusively as a dsDNA complex with plus strand DNA. The dsDNA serves as a template for replication and transcription (Hanley-Bowdoin et al., 1999), whereas plus strand DNA (ssDNA) is also encapsidated into virions. The FISH probes have the same polarity as the mRNA transcripts, so they do not cross-hybridize with viral RNA. The probes were co-synthetically labeled, thereby forming a single batch of uniformly labeled probes suitable for repeated experiments and signal quantification.

Fig. 2. Preservation of cellular and subcellular morphology following FISH. Vibratome-sectioned leaf material was immobilized in polyacrylamide and subjected to FISH and 3-D, multiple wavelength deconvolution microscopy. The DAPI, FITC, and Texas Red images are shown as blue, green and red, respectively. (A,B) Through-focus projections of 3-D image data after FISH with the AM + BM probe. Similarly oriented upper portions of leaf sections are shown for healthy control (A) and TGMV-infected (B) material. (C-E) Image projections from a single 3-D data stack taken from a TGMV-infected leaf. Chromosomal DNA is visualized in the DAPI channel (C), cellular autofluorescence in the FITC channel (D) and geminivirus DNA in the Texas Red channel (E). The healthy nucleus (single arrow) does not show Texas Red signals above background, whereas the infected nucleus (double arrow) is enlarged and contains numerous bright subdomains.
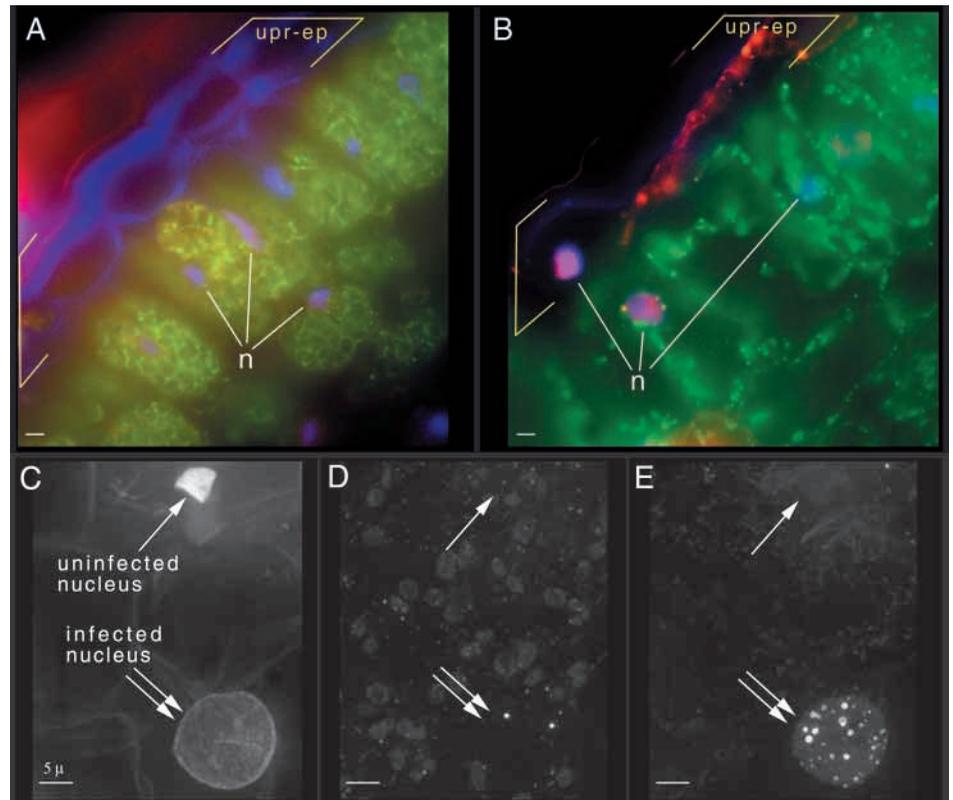
Geminivirus DNA is centrally located in infected nuclei

To determine whether viral DNA is localized in specific compartments or dispersed throughout infected nuclei, we performed 3-D FISH using probes corresponding to TGMV minus strands (AM and BM). These oligonucleotides hybridize with plus-strand viral DNA, found in both ssDNA and dsDNA. Our experiments detected a variety of accumulation patterns for TGMV DNA (Fig. 3A-E). FISH signals (Fig. 3, Texas Red rows) were limited to nuclei and ranged from uniform labeling (Fig. 3D) to conspicuous intranuclear compartments (Fig. 3B,C,E). A combination of the dispersed and compartmentalized patterns was also observed (Fig. 3A). The number and appearance of viral DNA compartments also varied from one large subdomain (Fig. 3B) to numerous smaller subdomains (Fig. 3A,E) or a combination of one large and several small subdomains (Fig. 3C). DAPI images revealed that total DNA in infected nuclei was concentrated at the nuclear periphery (Fig. 3A,B,D) and was sometimes fibrous in appearance (Fig. 3C,D). In Fig. 3A, the nuclear envelope appeared to invaginate deep into the nucleus.

The nucleus in Fig. 3B contained a single large inclusion in its center. This intranuclear compartment occupied 15% of the total nuclear volume and contained 39% of the total nuclear Texas red fluorescence counts (see Table 1). Despite the appearance of the image projections, we found that the intranuclear compartments, when pooled, were always less
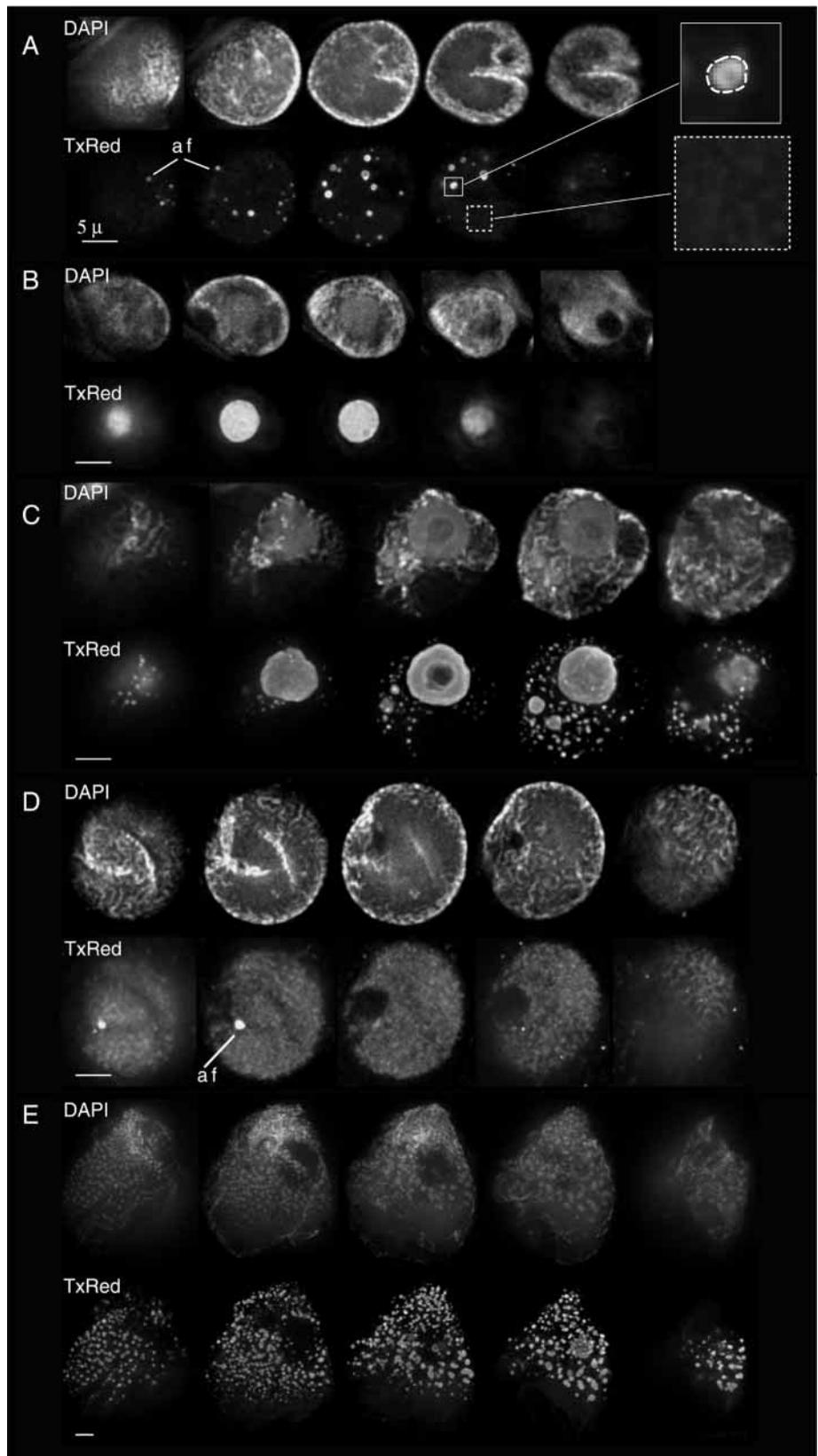

Fig. 3. Viral DNA is localized to discrete intranuclear compartments in infected nuclei. 3-D FISH was performed as described for Fig. 2. Gray-scale sequential projections of total DNA (DAPI) and corresponding Texas Red (TxRed)-labeled viral DNA (AM + BM probes) are shown for five representative, infected nuclei. The 3-D data subsets containing individual whole nuclei (40-60 optical sections) were converted to a series of five sequential projections, each with an effective focal plane depth of 1/5 the nucleus (~1.5-2.7 µm each). DAPI images for some nuclei show chromatin that is fibrous in appearance and usually concentrated near the nuclear periphery (C,D). Bright spots that fluoresce in both the FITC and Texas Red channels are thought to represent autofluorescence (af). The inset (A, far right) shows the outline of an intranuclear compartment (dashed circle) and a close-up of the diffuse staining (dashed box) between the bright compartments. Nuclei in A-D are shown at the same magnification. (E) A very large nucleus at relatively reduced magnification. Bars, 5 µm.

Table 1. Volume and relative intensity of intranuclear compartments stained by FISH for individual nuclei

Nucleus dataset‡	Probes	Total nuclear volume (μm^3)	Viral intranuclear compartments*				Chromatin fibers evident
			Number	Summed volume (μm^3)	% Nuclear volume	% Total counts in viral DNA compartments§	
1u3a.s01	AM+BM	107	(Uninfected)				No
1u3a.s02 (3A)	AM+BM	1534	39	14.8	1	4	Yes
1u3b.s01	AM+BM	379	(Uninfected)				No
1u3b.s02 (3B)	AM+BM	887	1	136.4	15.4	39	No
1u3b.s03	AM+BM	1326	1	191.6	14.4	37	No
1u3c.s01 (3C)	AM+BM	2181	4	389.8	17.9	45	Yes
1u3d.s01 (3E)	AM+BM	16055	>510	n.d.	n.d.	n.d	Unclear
1u3e.s01 (3D)	AM+BM	1967	0	0	0	0	Yes
2u3a.s01 (4A)	AP+BP	790	1	18.2	2.3	17	No
2u3a.s02 (4B)	AP+BP	768	1	4.1	0.5	2	No
2u3b.s01 (4C)	AP+BP	2643	34	345.7	13.1	37	Yes

*Compartments refer to the discrete, subnuclear, spherical entities that are brightly stained by FISH. The spatial and quantitative data were obtained from 3-D models of the whole nucleus and internal compartments (see Materials and Methods).

‡Each row represents a single nucleus with the corresponding figure and panel indicated in parentheses.

§Integrated intensities were determined for all the intranuclear compartments within a given nucleus with the exception of 1u3c.s01 in which only the four largest compartments were modeled and used. To normalize counts across from different experiments and different samples on the same slides, the counts in the Texas Red or rhodamine channels were calculated as follows; [(total integrated counts within the nucleus or the sum of subnuclear compartments)/(seconds of exposure)(Z-focal step size)].

than half of the total nuclear staining. Therefore viral DNA is not located exclusively in these compartments. This single, large inclusion type of labeling was detected in more than half of infected cells. In many cases, the compartments appeared to have substructure characterized by more intense labeling at the outer edges (Fig. 3C). We were unable to determine whether the hollowed appearance of FISH-stained compartments reflected true substructure or uneven staining related to probe accessibility or hybridization.

Less typical patterns of viral DNA accumulation are shown in Fig. 3D and E. The nucleus in Fig. 3D displayed abundant but diffuse DNA labeling. In Fig. 3E, the nucleus was over twice the diameter of most infected nuclei, had a lower intensity of DAPI staining at its margin and contained more than 300 discrete foci of Texas red fluorescence.
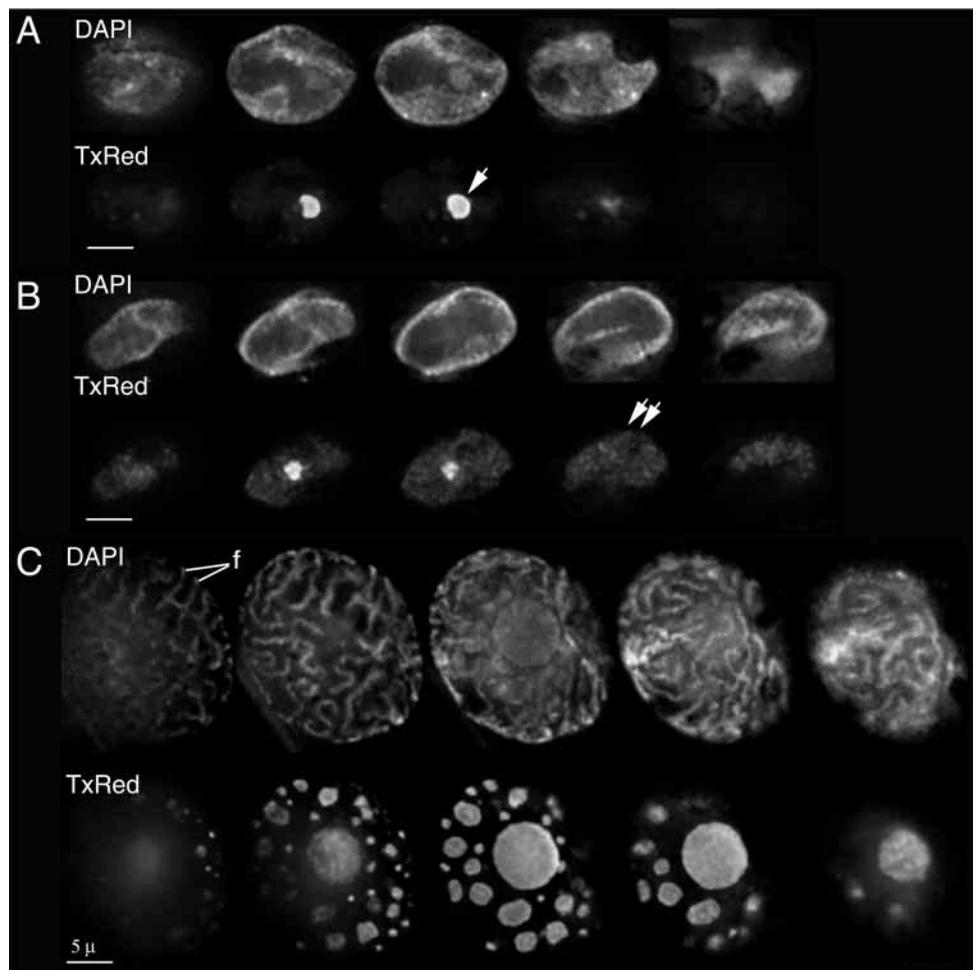

Fig. 4. dsDNA also localizes to intranuclear compartments. 3-D FISH images were collected and displayed as described for Fig. 3. DAPI and corresponding Texas Red images for representative TGMV-infected nuclei probed with plus-strand FISH probes, AP + BP. Two of the examples shown (A and B) were from adjacent cells, and the FISH signals show a bright subdomain (single arrow) amongst a more diffuse nuclear staining (double arrow). (C) Large infected nucleus shows FISH signals limited to bright subdomains, uniformly spaced and of variable sizes. DAPI image for this nucleus shows a striking condensation of chromatin into discrete fibers resembling mitotic prophase chromosomes.

Both plus and minus strand DNA localize to intranuclear compartments

Plus and minus strand DNA synthesis are separable processes in rolling circle replication, the mechanism used by geminiviruses to duplicate their genomes (Laufs et al., 1995; Saunders et al., 1991). Consequently, viral ssDNA may not be produced in or localized to the same nuclear compartments as dsDNA. It was not possible to visualize viral ssDNA specifically because FISH analysis was performed under denaturing conditions such that probes corresponding to TGMV minus-strand DNA labeled both ssDNA and dsDNA. When FISH probes derived from plus-strand DNA sequence were used (Fig. 4), they showed that the accumulation patterns for minus strand DNA alone resembled those seen for total DNA (Fig. 3). Because the accumulation of ssDNA is much greater than that of dsDNA, minus strand probe signal was expected to reflect primarily ssDNA accumulation. The intranuclear compartments displayed similar fluorescence intensities with the minus- and plus-strand probes (data not shown), suggesting that the compartments contained significant levels of dsDNA. In addition, the majority of probe hybridizing to dsDNA was found throughout the nucleus (Table 1), not preferentially within the bright intranuclear compartments. Together these results suggested that, under our FISH conditions, plus strand and minus strand DNA localize similarly in the nucleus and that the intranuclear compartments do not simply reflect inclusion bodies of viral particles.

Experiments using FISH probes for both minus and plus strand DNA did not detect any cells that contained predominately ssDNA, indicative of cells at late stages of infection no longer undergoing viral replication or transcription (data not shown). Such cells might have been detected at a later time. However, all enlarged nuclei that were visualized showed abundant FISH signal with both plus and minus strand probes. The results strongly suggest that

viral dsDNA does not turn over during late stages of infection even though it is no longer required as template.

No Texas red staining was detected in the cytoplasm of infected cells, perhaps because the sensitivity of detection of the oligonucleotides was not sufficient to detect cytoplasmic viral DNA. Alternatively, the form of viral DNA that moves through cells may associate with a structure that prevents access by the probes, or cytoplasmic viral DNA may not have been well fixed and may have been extracted by the FISH protocol.

Nuclear volume increases after infection

Nuclei in healthy mature leaf cells are typically adjacent to the plasma membrane. Upon infection, nuclei enlarge and move to the cell center, analogous to the morphological changes often associated with a return to the meristematic state. To further characterize the nuclear changes mediated by geminivirus infection, we measured the total nuclear volume and compared it to the volume of viral DNA compartments. Table 1 shows nuclear dimensions from infected and uninfected nuclei probed with minus- and plus-strand oligonucleotides. The average increase was about 6-fold but individual nuclei showed from
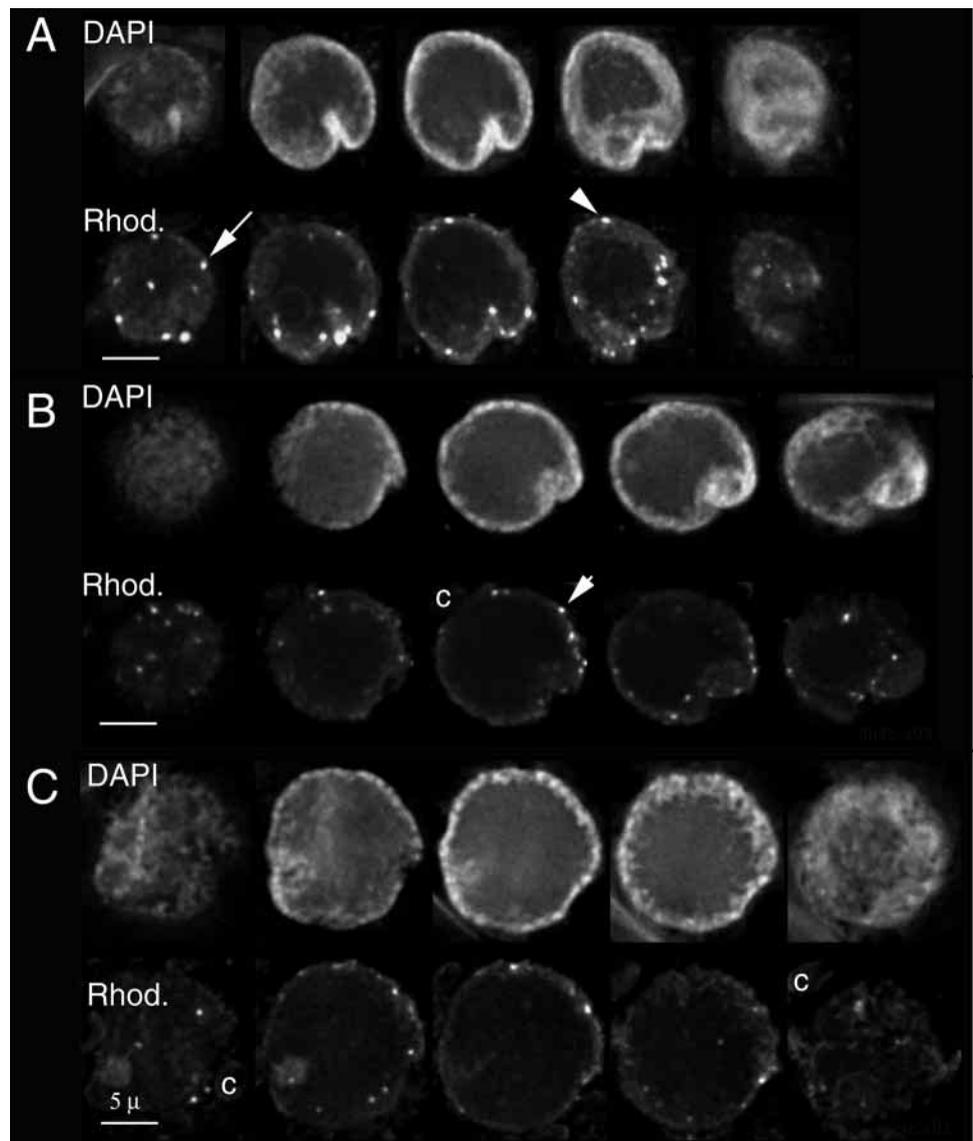

Fig. 5. 3-D GISH images from *N. benthamiana* genomic DNA probes. DAPI (DAPI) and corresponding rhodamine (Rhod.) images for representative TGMV-infected nuclei probed with rhodamine-dUTP-labeled *N. benthamiana* total DNA. Five-part sequential projection series were prepared and shown as described in Fig. 3. DAPI images show peripheral concentration of chromatin. Rhodamine images also show peripheral concentration of GISH signals with numerous small bright spots (arrow). Autofluorescent chloroplasts are indicated (c).

2- to 24-fold increases. Infected and healthy nuclei in adjoining spongy mesophyll cells showed a 14-fold variation in volume (Table 1, cf. datasets 1u3a.s01 and 1u3a.s02).

The relative volume occupied by the viral DNA compartments varied in different nuclei from less than 1% to about 18%. Although viral DNA appeared to occupy most of the volume of some nuclei (e.g. Fig. 2B), actual measurements showed that this illusion was a projection artifact due in part to the nature of sphere volumes. The total amount of probe fluorescence varied substantially from nucleus to nucleus, perhaps as a reflection of different stages of infection or varying degrees of success in establishing and maintaining viral DNA infection in different nuclei. Because some of the plus-strand DNA is encapsidated and may differ from unencapsidated DNA in its accessibility to probe, the relative intensities of plus- and minus-strand probes (e.g. Table 1) could not be directly compared.

Host chromatin is concentrated at the nuclear periphery in infected cells

DAPI staining of TGMV-infected nuclei suggested that host chromatin was located at the periphery (Figs 3-4). To verify that host DNA was redistributed, we labeled total *N. benthamiana* genomic DNA with rhodamine and used it for genomic in situ hybridization (GISH) of infected tissue sections. Fig. 5 shows DAPI and *N. benthamiana* GISH signals for nuclei that displayed clear morphological signs of viral infection. The GISH signals, like the DAPI fluorescence, were brighter around the nuclear periphery, but the GISH signals also contained numerous small, bright foci (Fig. 5, arrows) with punctate staining patterns in the outer shell of chromatin. These bright spots, which occurred at a frequency of approximately 30-40 per nucleus, may have corresponded to centromeric regions. Centromeres contain repeated sequences that would be expected to stain intensely because of their relative abundance as probe and target. *N. benthamiana* has 38 centromeres in diploid somatic cells (Japan Tobacco, 1990) similar to the number of bright foci per nucleus.

To map the relative positions of the host and viral DNA more precisely with respect to the nuclear envelope, we constructed a plot to assess the co-localization of DAPI and rhodamine signals. Fig. 6 shows intensity plotted as a function of position
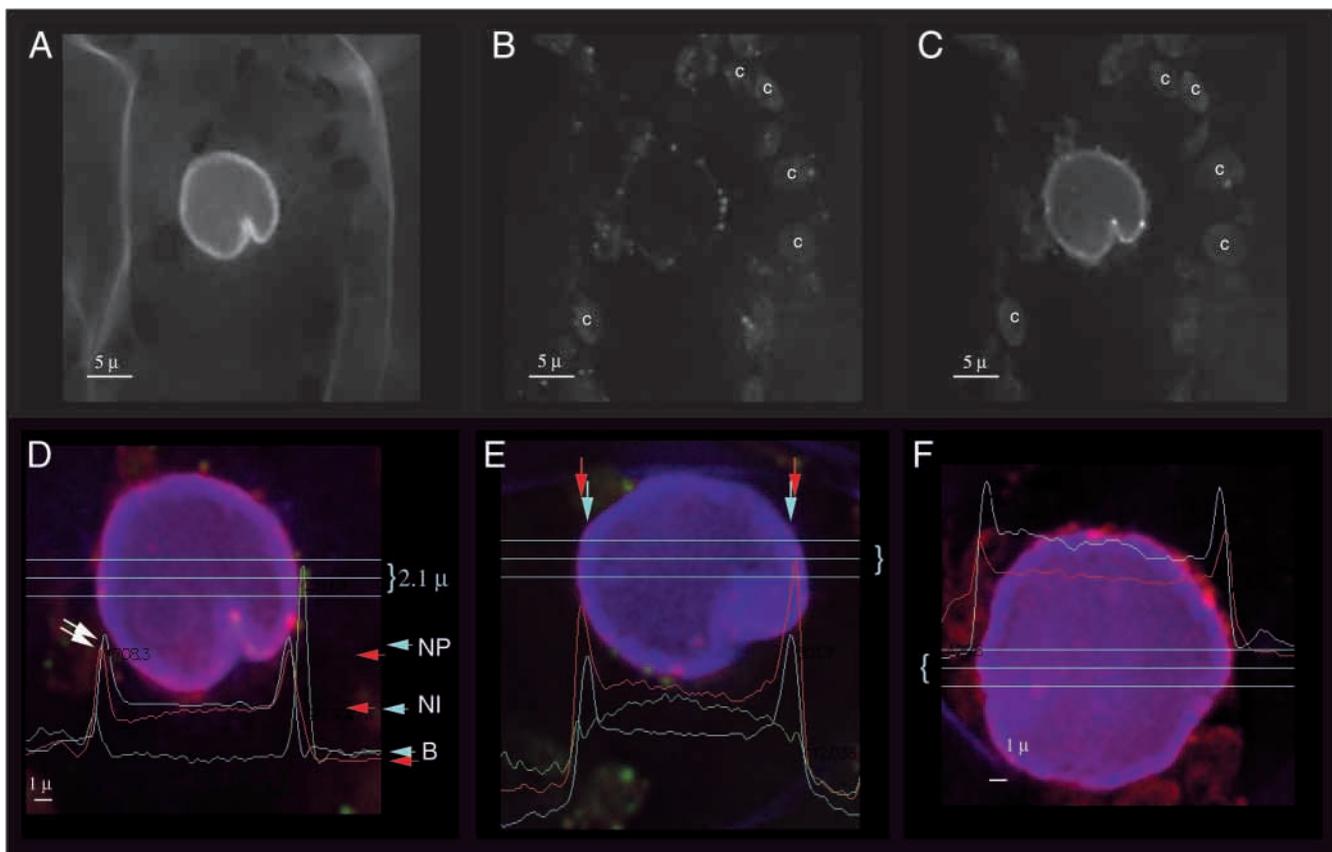

Fig. 6. Peripheral DAPI staining co-localizes with host DNA. A 3 μm projection through the middle of a TGMV-infected nucleus is shown for each of three wavelengths, (A) DAPI (B) FITC (autofluorescence) and (C) rhodamine, showing fluorescence from *N. benthamiana* GISH probe as described for Fig. 5. Chloroplasts are indicated (c). (D-F) Colocalization of DAPI and host DNA GISH signals. Relative intensity profiles are plotted for a 2.1 μm tall band across the nucleus (blue horizontal bands). Cyan, red, and blue tracings show average pixel intensity for the DAPI, FITC, and rhodamine images, respectively. Height of the line tracing is directly proportional to the average intensity of the column of voxels (X Y Z of 1 pixel wide (X), 19 pixels tall (Y, 2.1 μm) and 8-10 pixels deep (~3 μm Z projection)). (D-F) Three different representative nuclei. (D) Overlapping peaks (arrows) across the X axis demonstrate co-localization of DAPI and rhodamine signals. Signal peaks at the nuclear periphery (NP) are greater than signals across the nuclear interior (NI) which are greater than background signals (B) outside the nucleus. In the FITC images, a ring of autofluorescence around the nucleus is also observed, but the peaks are outside of the DAPI peaks (green tracings). The positions of the peripheral peaks are indicated in E with arrows above the nucleus.

within a rectangular column through the center of an infected nucleus. The DAPI-stained peripheral shell of chromatin colocalized with the *N. benthamiana* GISH rhodamine signals in very similar positions at the nuclear periphery (Fig. 6D, NP). The fluorescein image (green, green scan Fig. 6D,E) showed autofluorescence probably derived from plastids that frequently are attached to the cytoplasmic face of the nuclear envelope. A careful inspection of the nucleus in Fig. 6A-C revealed that speckled autofluorescence surrounding the nucleus in Fig. 6B was from outside of the nucleus (see Fig. 6 legend).

Modification of host chromatin

Some mammalian DNA viruses alter cell cycle controls to cause the up-regulation of DNA replication factors (Nevins, 1992). Many of these viruses are oncogenic and are propagated through mitosis (Skiadopoulos and McBride, 1998). In contrast, TGMV infection does not result in tumor formation, but a significant number of infected nuclei contained condensed chromatin characteristic of cells in early prophase. In Fig. 4C, chromosome condensation was detected at the margin of a TGMV-infected nucleus. The step-through images showed numerous foci of viral DNA accumulation within the nucleus. Although some chromatin fibers appeared to traverse the interior of the nucleus, inspection of several different nuclei revealed that the chromatin fibers almost always were limited to the periphery of the nucleus.

Two projections of the DAPI image of a TGMV-infected nucleus with several foci of viral DNA within condensed chromatin are shown in Fig. 7. Condensed chromatin was never observed in differentiated cells of mock-inoculated plants. Although condensation was observed frequently, we did not see infected cells that progressed beyond prophase. The data in Table 1 showed that nuclei with large volumes and high levels of viral DNA accumulation are more likely to contain condensed chromatin. These observations are consistent with the idea that chromosome condensation occurs late in infection, possibly after viral DNA replication is completed.

We saw chromatin condensation in cells of the leaf, stem pith and cortex and midvein parenchyma but never saw chromosome condensation in cells unless they contained viral
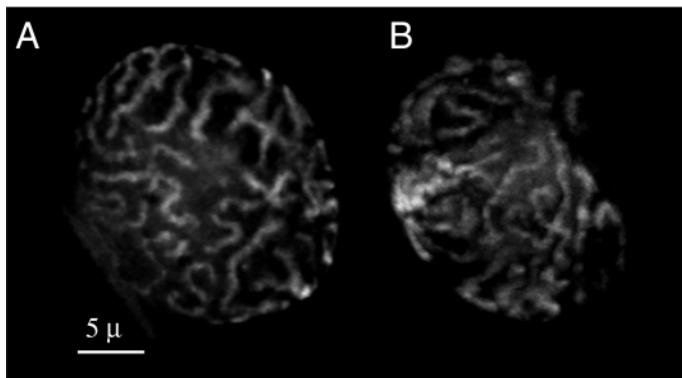
DNA. Together, these observations indicated that chromatin condensation depends on geminivirus infection and does not display cell type specificity. Occasionally we observed cells with mitotic figures near the stem vascular tissue. These cells did not contain viral DNA and were also present in equivalent healthy tissue, indicating that the meiotic figures were not related to geminivirus infection.

## Coat protein expression increases the number and size of viral DNA foci

TGMV ssDNA is packaged into viral particles in plant nuclei (Hamilton et al., 1983). We used a combination of FISH and indirect immunolabeling of coat protein to determine whether viral DNA foci represented encapsidated DNA. The panels shown in Fig. 8 used BP, a FISH probe hybridizing to dsDNA only from the B component. As shown in Fig. 8, most nuclei stained positive for both viral DNA and coat protein, but in some nuclei, viral DNA signals were very bright whereas coat protein could not be detected (arrows, Fig. 8A,C). Coat protein synthesis and association with replication compartments is likely to be regulated, occurring at specific time points in the infection process. This conclusion is consistent with our observation that detectable levels of coat protein were seen only in cells with high levels of viral DNA (compare Fig. 8A,C). It is also possible that a small number of cells with high levels of viral DNA never develop well-defined inclusion bodies.

To determine whether the coat protein plays a role in the accumulation of dsDNA, we examined FISH signals from a mutant TGMV capable of infection but lacking a functional coat protein gene (Fig. 8D-F). A previous study showed that viral DNA from this mutant showed reduced accumulation of dsDNA and undetectable amounts of ssDNA as determined by DNA gel blot hybridization of systemically infected tissues (Pooma et al., 1996). The amount of viral dsDNA staining was greatly reduced in this coat protein mutant (compare Fig. 8C,F), but small compartments were detected in the mutant infection (Fig. 9), suggesting that initial formation of viral DNA compartments does not require coat protein. Chromatin condensation was also observed in some infected nuclei when the coat protein was absent (Fig. 9). In *N. benthamiana*, a small proportion of cells has two nuclei naturally, and the nuclei shown in Fig. 9 are from a single cell. Chromatin condensation is never observed in these cells unless they are infected with TGMV.

DISCUSSION

Earlier studies showed that TGMV particles accumulate as large crystalline arrays in the nuclei of infected plant cells (Rushing et al., 1987). Immunohistochemical experiments demonstrated that the viral replication proteins, AL1 and AL3, also localize to nuclei of infected cells (Nagar et al., 1995). We have extended these studies by directly visualizing TGMV and plant DNA within nuclei of cells that have been carefully fixed and stained to preserve chromatin and nuclear architecture. Our experiments showed that viral DNA accumulates in discrete compartments whose number and size vary between nuclei. The formation of the intranuclear compartments did not depend on virus encapsidation, suggesting that they may act as foci for

Fig. 7. TGMV-infection can induce chromatin condensation into prophase-like fibers. A projection of DAPI image from a nucleus shows the first 14 (A) and last 14 (B) optical sections of the same nucleus. The viral FISH signals are not shown, but can be seen in Fig. 4C. Discrete, well separated fibers are evident.

Fig. 8. High numbers of viral DNA compartments require coat protein expression. Leaf tissue from systemically infected *N. benthamiana* was fixed 11 d.p.i. and processed for FISH using Texas Red-labeled oligonucleotide probes for minus strand detection (BP) and subsequently processed for coat protein localization by indirect immunofluorescence with an Alexa 488-conjugated secondary antibody. A-C, tissue infected with wt TGMV; (D-F) similar tissue infected with a coat protein mutant TGMV. (A,D) Alexa-488 fluorescence (green) showing coat protein localization; (B,E) triple fluorescence showing DAPI staining for DNA (blue), Texas Red fluorescence of the viral DNA probe (red), and Alexa 488 fluorescence of the coat protein conjugates (green, colocalized with red viral DNA signal and DAPI to produce white). (C,F) Texas Red fluorescence of viral DNA probe. Bar, 100 μm.
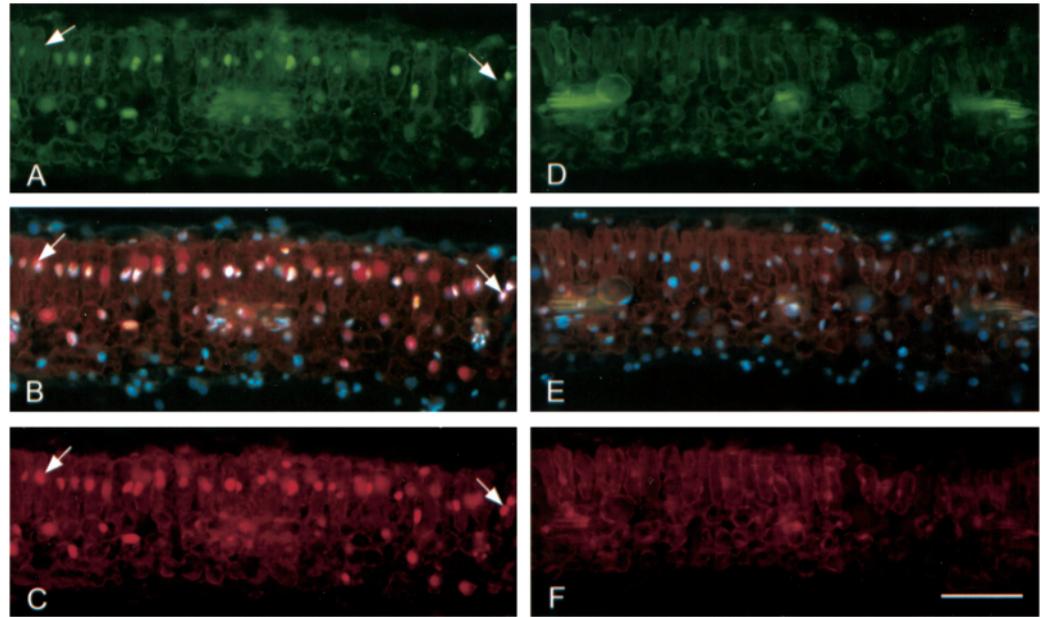
virus replication and transcription. We also detected significant accumulation of TGMV DNA throughout the interior of the nucleus. In contrast, plant DNA relocalized to the nuclear periphery and frequently occurred as condensed chromatin characteristic of cells in prophase. Together, these results established that geminivirus infection alters nuclear architecture and may induce infected plant cells to reenter the cell cycle and progress to early mitosis.

We detected a variety of TGMV DNA accumulation patterns, ranging from diffuse nuclear labeling to large intranuclear compartments. Similarly, nuclear substructures are frequently associated with DNA virus infection in animal cells. Herpesvirus, adenovirus and papovavirus genomes are found at the periphery of intranuclear sites, designated nuclear

Fig. 9. Chromosome fibers are seen in coat protein mutant TGMV-infected nuclei. Tissue infected with the TGMV mutant was processed as described for Fig. 8. A single cell with two nuclei is shown with DAPI fluorescence on the left and Texas Red fluorescence, corresponding to viral DNA accumulation, on the right. Small compartments containing significant amounts of viral probe can be seen. Both nuclei show evidence of chromosome condensation. Bar, 10 μm.

domain 10 (ND10), that contain host proteins upregulated by interferon or associated with ubiquitin pathways (Ishov and Maul, 1996; Maul, 1998). Animal proteins associated with DNA replication, such as cyclin A, cdk2 and DNA methyltransferase, contain localization sequences that direct them to sites of DNA replication (Cardoso et al., 1993). Although the relationship between the intranuclear compartments in plant and animal cells is not known, their overall appearances and distributions are strikingly similar, suggesting that they may have similar roles during DNA virus infection. As more probes for nuclear and DNA replication proteins become available for plants, it will be possible to determine whether the intranuclear structures reflect aspects of nuclear architecture and eukaryotic viral DNA replication that are conserved across kingdoms.

The functional significance of the different TGMV DNA patterns is not clear. The asynchronous character of the infection process in plants is likely to result in different levels of viral DNA accumulation at the time of tissue fixation. The observed patterns of viral DNA accumulation may represent different stages of an ongoing process or may reflect inherent variability in plant nuclear structure or in the propensity of nuclei to support viral DNA replication. DNA replication foci have not been well characterized in plants, and it is unclear how endoreduplication affects the number or location of these structures. Plant nuclei show varying degrees of endoreduplication within and among tissues and unlike animal cells, which leave the cell cycle in G_1, plant cells can exit the cell cycle in G_1 or G_2 (Gendreau et al., 1998; Gilissen et al., 1994; Valente et al., 1998). The variation in viral DNA inclusion size may therefore be a reflection of the different resting states of individual nuclei at the time of infection.

Single large inclusions were the most common structures found in infected nuclei. If the smaller compartments represent earlier stages of infection and not a terminal stage, two models can be proposed for the infection process. One possibility is
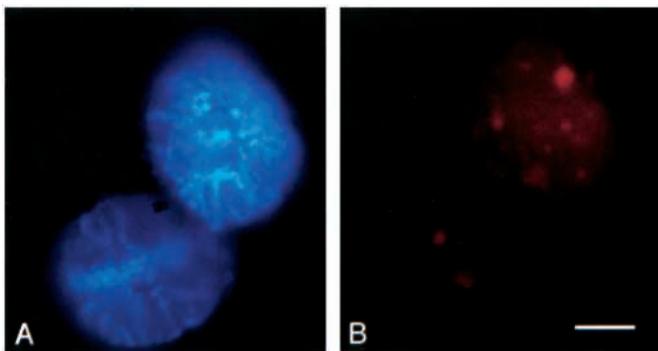
that the diffuse labeling (i.e. Fig. 4B) represents an early stage and that viral DNA (or particles) coalesces into compartments that increase in size as viral DNA is replicated and encapsidated. Alternatively, the diffuse staining may correspond to transcriptionally active dsDNA, whereas the highly fluorescent compartments may represent areas of ssDNA replication from double-stranded templates. Both ideas are supported by our results with the AR1 mutant. Previous studies showed that ssDNA accumulation is markedly reduced in mutants lacking a functional coat protein (Pooma et al., 1996). The FISH analysis of AR1-mutant infected leaf tissue demonstrated that discrete compartments containing high levels of viral DNA occurred at lower frequencies and were smaller in area. The coat protein is not required for the establishment of these compartments because some viral DNA was sequestered into brightly fluorescing areas in infections with a mutant virus lacking a functional coat protein gene (Fig. 9). These results suggested that initiation of plus-strand replication occurs in the absence of coat protein but that stabilization of ssDNA in specific compartments requires encapsidation. However, because the pattern of ssDNA could only be inferred by comparison of the labeling patterns of the minus-strand probe (hybridizing to total DNA) and plus-strand probe, we are unable to conclude whether ssDNA is restricted to specific compartments or, like dsDNA, occurs throughout the nucleus.

We did not observe markedly different patterns of dsDNA or total viral DNA accumulation in TGMV-infected plants. This result was surprising because of DNA gel blot data showing that TGMV ssDNA is at least 10-fold more abundant in infected plants (Rogers et al., 1989). In addition, a time course of TGMV replication during synchronous infection of tobacco protoplasts showed that the ratio of ssDNA to dsDNA rose between 18 and 48 hours (Brough et al., 1992). The FISH signal intensities of dsDNA detected in this study were similar to those of ssDNA and were therefore unexpected. This result suggests that encapsidated ssDNA was more difficult to detect than dsDNA, as would be expected from our fixation protocol, and our results were therefore skewed. The presence of dsDNA in all infected cells suggested that it does not turn over late in infection when it is no longer required as template for replication or transcription. Infected cells, most of which do not show visible signs of cell death (Nagar et al., 1995), may not have a mechanism for degrading the dsDNA. Alternatively, dsDNA may serve another function, for instance in movement, that requires its maintenance throughout the virus life cycle.

In TGMV-infected cells, plant chromosomal DNA moved to the nuclear margin (this study and see Rushing et al., 1987) and frequently displayed condensation (Fig. 7). In animal cells, condensed chromatin is caused by activation of a cyclin-dependent kinase, p34 cdc2, which phosphorylates chromatin components such as histone H1 during cell cycle progression (Koshland and Strunnikov, 1996). Recently, condensed chromatin was also correlated with histone phosphorylation in plants (Houban et al., 1999). Condensed chromatin in geminivirus-infected nuclei may therefore indicate cells that have been induced to reenter the cell cycle and progress to early mitosis. Mounting evidence supports this hypothesis, including geminivirus dependence on host DNA replication machinery and the induction of high PCNA levels in TGMV-infected cells

(Nagar et al., 1995). Normally plant DNA replication enzymes and factors, including PCNA, are only detectable in cycling cells (Benedetto et al., 1996; Kodama et al., 1991). Like mammalian DNA tumor viruses which are known to reprogram cell cycle controls, geminiviruses encode proteins that interact with plant homologues of retinoblastoma protein (Ach et al., 1997; Collin et al., 1996; Grafi et al., 1996; Xie et al., 1995), a negative regulator of cell cycle progression (Chow et al., 1996). Recent studies showed that impairment of the interaction between TGMV AL1 and retinoblastoma protein attenuates symptoms and limits tissue specificity of infection (L. Hanley-Bowdoin et al., unpublished results), thereby underscoring the importance of this interaction during the geminivirus infection process. It should be noted that chromosome structure is also altered and condensed in mammalian cells undergoing apoptosis, but this is a transient phase related to rapid proteolysis of nuclear matrix proteins (Hendzel et al., 1998; Oberhammer et al., 1994). Given the transitory character of chromatin condensation during apoptosis and the absence of significant cell death of geminivirus-infected cells, we believe that the TGMV-induced condensation described here is different from that induced by programmed cell death.

Even though the majority of TGMV-infected cells contained condensed chromatin characteristic of cells in prophase, we never saw evidence for metaphase or other stages of cell division. In addition, tumors are not associated with TGMV infection in *N. benthamiana*, suggesting that cell cycle progression is blocked in infected cells. To our knowledge, this is the first report of such a block associated with viral DNA infection. One possible explanation for a cell cycle arrest at prophase is that TGMV infections actively prevent plant cells from continuing through mitosis by an unknown mechanism. Alternatively, unlike mammalian DNA tumor viruses, TGMV infection may be unable to induce all the signals necessary for transit through mitosis. Interestingly, the regulatory mechanisms that control the G_2/M transition in plants appear to be less similar to those in animals than are those regulating G_1/S progression (Inze et al., 1999). The absence of a necessary signal for completion of cell division is also supported by the observation that beet curly top virus, a member of the curto-geminivirus family, causes hyperplasia in *N. benthamiana* through the action of its C4 protein (Latham et al., 1997). Interestingly, bean yellow dwarf virus, a mastre-geminivirus that also induces ectopic cell division, contains a functional C4 gene (Liu et al., 1997, 1999). In contrast, TGMV does not encode a functional C4 homologue and, thus, may not be able to drive plant cells through mitosis. As more plant cell cycle-specific markers become available, it will be possible to characterize better the interactions between geminiviruses and plant cell cycle regulators and to determine why some viruses can induce cell division in their hosts whereas others are associated with an arrest in early mitosis.

REFERENCES

Ach, R. A., Durfee, T., Miller, A. B., Taranto, P., Hanley-Bowdoin, L., Zambryski, P. C. and Gruissem, W. (1997). RRB1 and RRB2 encode maize retinoblastoma-related proteins that interact with a plant D-type cyclin and geminivirus replication protein. *Mol. Cell Biol.* **17**, 5077-5086.

Bass, H. W., Marshall, W. F., Sedat, J. W., Agard, D. A. and Cande, W. Z. (1997). Telomeres cluster de novo before the initiation of synapsis: a three-dimensional spatial analysis of telomere positions before and during meiotic prophase. *J. Cell Biol.* **137**, 5-18.

Belmont, A. S., Braunfeld, M. B., Sedat, J. W. and Agard, D. A. (1989). Large-scale chromatin structural domains within mitotic and interphase chromosomes in vivo and in vitro. *Chromosoma* **98**, 129-143.

Benedetto, J. P., Echchaoui, R., Plissonneau, J., Laquel, P., Litvak, S. and Castroviejo, M. (1996). Changes of enzymes and factors involved in DNA synthesis during wheat embryo germination. *Plant Mol. Biol.* **31**, 1217-1225.

Bisaro, D. M., Hamilton, W. D. O., Coutts, R. H. A. and Buck, K. W. (1982). Molecular cloning and characterization of the two DNA components of tomato golden mosaic virus. *Nucl. Acids Res.* **10**, 4913-4922.

Bravo, R., Frank, R., Blundell, P. A. and MacDonald-Bravo, H. (1987). Cyclin/PCNA is the auxilliary protein of DNA polymerase-δ. *Nature* **326**, 515-517.

Brough, C. L., Hayes, R. J., Morgan, A. J., Coutts, R. H. A. and Buck, K. W. (1988). Effects of mutagenesis in vitro on the ability of cloned tomato golden mosaic virus DNA to infect *Nicotiana benthamiana* plants. *J. Gen. Virol.* **69**, 503-514.

Brough, C. L. Sunter, G., Gardiner, W. and Bisaro, D. (1992). Kinetics of tomato golden mosaic virus replication and coat protein promoter activity in *Nicotiana tabacum* protoplasts. *Virology* **187**, 1-9.

Cardoso, M. C., Leonhardt, H. and Nadal-Ginard, B. (1993). Reversal of terminal differentiation and control of DNA replication: cyclin A and cdk2 specifically localize at subnuclear sites of DNA replication. *Cell* **74**, 979-992.

Chen, H., Swedlow, J. R., Grote, M. A., Sedat, J. W. and Agard, D. A. (1995). *The collection, processing, and display of digital three-dimensional images of biological specimens.* New York: Plenum Press.

Chen, H., Hughes, D. D., Chan, T.-A., Sedat, J. W. and Agard, D. A. (1996). IVE (Image Visualization Environment): a software platform for all three-dimensional microscopy applications. *J. Struct. Biol.* **116**, 56-60.

Chow, K. N. B., Starostik, P. and Dean, D. C. (1996). The rb family contains a conserved cyclin-dependent kinase-regulated transcriptional repressor motif. *Mol. Cell Biol.* **16**, 7173-7181.

Collin, S., Fernandezlobato, M., Gooding, P. S., Mullineaux, P. M. and Fenoll, C. (1996). The two nonstructural proteins from wheat dwarf virus involved in viral gene expression and replication are retinoblastoma-binding proteins. *Virology* **219**, 324-329.

de Bruyn Kops, A. and Knipe, D. M. (1994). Preexisting nuclear architecture defines the intranuclear location of herpesvirus DNA replication structures. *J. Virol.* **68**, 3512-3526.

Elmer, J. S., Sunter, G., Gardiner, W. E., Brand, L., Browning, C. K., Bisaro, D. M. and Rogers, S. G. (1988). *Agrobacterium*-mediated inoculation of plants with tomato golden mosaic virus DNAs. *Plant Mol. Biol.* **10**, 225-234.

Fontes, E. P. B., Gladfelter, H. J., Schaffer, R. L., Petty, I. T. D. and Hanley-Bowdoin, L. (1994). Geminivirus replication origins have a modular organization. *Plant Cell* **6**, 405-416.

Gardiner, W. E., Sunter, G., Brand, L., Elmer, J. S., Rogers, S. G. and Bisaro, D. M. (1988). Genetic analysis of tomato golden mosaic virus: The coat protein is not required for systemic spread or symptom development. *EMBO J.* **7**, 899-904.

Gendreau, E., Hofte, H., Grandjean, O., Brown, S. and Traas, J. (1998). Phytochrome controls the number of endoreduplication cycles in the *Arabidopsis thaliana* hypocotyl. *Plant J.* **13**, 221-230.

Gilissen, L. J. W., Vanstaveren, M. J., Hakkert, J. C., Smulders, M. J. M., Verhoeven, H. A. and Creemersmolenaar, J. (1994). The competence of cells for cell division and regeneration in tobacco explants depends on cellular location, cell cycle phase and ploidy level. *Plant Sci.* **103**, 81-91.

Grafi, G., Burnett, R. J., Helentjaris, T., Larkins, B. A., DeCaprio, J. A.,

Sellers, W. R. and Kaelin, W. G., Jr. (1996). A maize cDNA encoding a member of the retinoblastoma protein family: involvement in endoreduplication. *Proc. Nat. Acad. Sci. USA* **93**, 8962-8967.

Hamilton, W. D. O., Bisaro, D. M., Coutts, R. H. A. and Buck, K. W. (1983). Demonstration of the bipartite nature of the genome of a single-stranded DNA plant virus by infection with the cloned DNA components. *Nucl. Acids Res.* **11**, 7387-7396.

Hamilton, W. D. O., Stein, V. E., Coutts, R. H. A. and Buck, K. W. (1984). Complete nucleotide sequence of the infectious cloned DNA components of tomato golden mosaic virus: Potential coding regions and regulatory sequences. *EMBO J.* **3**, 2197-2205.

Hanley-Bowdoin, L., Settlage, S. B., Orozco, B. M., Nagar, S. and Robertson, D. (1999). Geminiviruses – models for plant DNA replication, transcription and cell cycle regulation. *Curr. Biol.* **18**, 71-106.

Hendzel, M. J., Nichioka, W. K., Raymond, Y., Allis, C. D., Bazett-Jones, D. P. and Th'ng, J. P. H. (1998). Chromatin condensation is not associated with apoptosis. *J. Biol. Chem.* **38**, 24470-24478.

Hiraoka, Y., Swedlow, J. R., Paddy, M. R., Agard, D. A. and Sedat, J. W. (1991). Three-dimensional multiple wavelength fluorescence microscopy for the structural analysis of biological phenomena. *Semin. Cell Biol.* **2**, 153-165.

Houban, A., Wako, T., Furushima-Shimogawara, R., Presting, G., Kunzel, G., Schubert, I. and Fukui, K. (1999). The cell cycle dependent phosphorylation of histone H3 is correlated with the condesation of plant mitotic chromosomes. *Plant J.* **18**, 675-679.

Inze, D., Gutierrez, C. and Chua, N. H. (1999). Trends in plant cell cycle research. *Plant Cell* **11**, 991-994.

Ishov, A. M. and Maul, G. G. (1996). The periphery of nuclear domain 10 (ND10) as site of DNA virus deposition. *J. Cell Biol.* **134**, 815-826.

Ishov, A. M., Stenberg, R. M. and Maul, G. G. (1997). Human cytomegalovirus immediate early interaction with host nuclear structures: definition of an immediate transcript environment. *J. Cell Biol.* **138**, 5-16.

Japan Tobacco Inc. (1990). *Illustrated Book of the Genus* Nicotiana. Japan Tobacco Inc., Plant Breeding and Genetics Research Laboratory.

Kelman, Z. (1997). PCNA: structure, functions and interactions. *Oncogene* **14**, 629-640.

Kim, K., Shcok, T. and Goodman, R. (1978). Infection of *Phaseolus vulgaris* by bean golden mosaic virus: ultrastructural aspects. *Virology* **89**, 22-33.

Kodama, H., Ito, M., Ohnishi, N., Suzuka, I. and Komamine, A. (1991). Molecular cloning of the gene for plant proliferating-cell nuclear antigen and expression of this gene during the cell cycle in synchronized cultures of *Catharanthus roseus* cells. *Eur. J. Biochem.* **197**, 495-503.

Koshland, D. and Strunnikov, A. (1996). Mitotic chromsome condensation. *Annu. Rev. Cell Dev. Biol.* **12**, 305-333.

Latham, J. R., Saunders, K., Pinner, M. S. and Stanley, J. (1997). Induction of plant cell division by beet curly top virus gene C4. *Plant J.* **11**, 1273-1283.

Laufs, J., Jupin, I., David, C., Schumacher, S., Heyraudnitschke, F. and Gronenborn, B. (1995). Geminivirus replication: genetic and biochemical characterization of Rep protein function, a review. *Biochimie* **77**, 765-773.

Liu, L., vanTonder, T., Pietersen, G., Davies, J. W. and Stanley, J. (1997). Molecular characterization of a subgroup I geminivirus from a legume in South Africa. *J. Gen. Virol.* **78**, 2113-2117.

Liu, L., Saunders, K., Thomas, C. L., Davies, J. W. and Stanley, J. (1999). Bean yellow dwarf virus RepA, but not Rep, binds to maize retinoblastoma protein, and the virus tolerates mutations in the consensus binding motif. *Virology* **256**, 270-279.

Maul, G. G. (1998). Nuclear domain 10, the site of DNA virus transcription and replication. *BioEssays* **20**, 660-667.

Nagar, S., Pedersen, T. J., Carrick, K. M., Hanley-Bowdoin, L. and Robertson, D. (1995). A geminivirus induces expression of a host DNA synthesis protein in terminally differentiated plant cells. *Plant Cell* **7**, 705-719.

Nevins, J. (1992). E2F - a link between the Rb tumor suppressor protein and viral oncoproteins. *Science* **258**, 424-429.

Oberhammer, F. A., Hochegger, K. and Froschl, G. (1994). Chromatin condensation during apoptosis is accompanied by degradation of lamin A+B, without enhanced activation of cdc2 kinase. *J. Cell Biol.* **126**, 827-837.

Pooma, W., Gillette, W. K., Jeffrey, J. L. and Petty, I. T. D. (1996). Host and viral factors determine the dispensability of coat protein for bipartite geminivirus systemic movement. *Virology* **218**, 264-268.

Rogers, S. G., Bisaro, D. M., Horsch, R. B., Fraley, R. T., Hoffman, N. L.,

Brand, L., Elmer, J. S. and Lloyd, A. M. (1986). Tomato golden mosaic virus A component DNA replicates autonomously in transgenic plants. *Cell* **45**, 593-600.

Rogers, S. G., Elmer, J. S., Sunter, G., Gardiner, W. E., Brand, L., Browning, C. K. and Bisaro, D. M. (1989). Molecular genetics of tomato golden mosaic virus. In *Molecular Biology of Plant-Pathogen Interactions* (ed. B. Staskawicz, P. Ahlquist and O. Yoder), pp. 199-215. New York: Alan R. Liss.

Rushing, A. E., Sunter, G., Gardiner, W. E., Dute, R. R. and Bisaro, D. M. (1987). Ultrastructural aspects of tomato golden mosaic virus infection in tobacco. *Phytopathology* **77**, 1231-1236.

Saunders, K., Lucy, A. and Stanley, J. (1991). DNA forms of the geminivirus African cassava mosaic virus consistent with a rolling circle mechanism of replication. *Nucl. Acids Res.* **19**, 2325-2330.

Skiadopoulos, M. H. and McBride, A. A. (1998). Bovine papillomavirus type 1 genomes and the E2 transactivator protein are closely associated with mitotic chromatin. *J. Virol.* **72**, 2079-2088.

Sunter, G., Gardiner, W. E., Rushing, A. E., Rogers, S. G. and Bisaro, D. M. (1987). Independent encapsidation of tomato golden mosaic virus A component DNA in transgenic plants. *Plant Mol. Biol.* **8**, 477-484.

Uprichard, S. L. and Knipe, D. M. (1997). Assembly of herpes simplex virus replication proteins at two distinct intranuclear sites. *Virology* **229**, 113-125.

Valente, P., Tao, W. H. and Verbelen, J. P. (1998). Auxins and cytokinins control DNA endoreduplication and deduplication in single cells of tobacco. *Plant Sci*. **134**, 207-215.

Xie, Q., Suarezlopez, P. and Gutierrez, C. (1995). Identification and analysis of a retinoblastoma binding motif in the replication protein of a plant DNA virus: requirement for efficient viral DNA replication. *EMBO J.* **14**, 4073-4082.